Three-dimensional centrifuge and numerical modeling of the interaction between perpendicularly crossing tunnels

Charles W. W. Ng, Thayanan Boonyarak and David Mašín

Crown-author: Dr C. W. W. Ng

Chair Professor, Department of Civil and Environmental Engineering, Hong Kong University of Science and Technology, Clear Water Bay, Kowloon, Hong Kong.
E-mail: cecwwng@ust.hk
Tel: 852-2358-8760
Fax: 852-2358-1534

Corresponding author: Mr T. Boonyarak

Research student, Department of Civil and Environmental Engineering, Hong Kong University of Science and Technology, Clear Water Bay, Kowloon, Hong Kong.
E-mail: thayanan@ust.hk
Tel: 852-6848-8574

Co-author: Dr D. Mašín

Associate Professor, Faculty of Science, Charles University in Prague, Albertov 6, 128 43 Prague 2, Czech Republic.
E-mail: masin@natur.cuni.cz
Tel: 420-2-2195-1552

Abstract: Tunnel driving inevitably induces changes in stress and deformation in the ground, which could cause ultimate and serviceability problems to an adjacent tunnel. The effects of induced stress on an existing tunnel and crossing-tunnel interaction are still not fully understood. In this study, a series of three-dimensional centrifuge tests were carried out to investigate the responses of an existing tunnel in sand to the excavation of a new tunnel perpendicularly underneath it. Three-dimensional tunnel advancement was simulated using a novel technique that considers the effects of both volume and weight losses. This novel technique involves using a "donut" to control volume loss and mimic soil removal in-flight. To improve fundamental understanding of stress transfer mechanism during the new tunnel advancement, measured results were back-analyzed three-dimensionally using the finite element method. The maximum measured settlement of the existing tunnel induced by the new tunnel constructed underneath was about 0.3% of tunnel diameter, which may be large enough to cause serviceability problems. The observed large settlement of the existing tunnel was caused not only by a sharp reduction in vertical stress at the invert but also by substantial overburden stress transfer at the crown. The section of the existing tunnel directly above the new tunnel was vertically compressed because the incremental normal stress on the existing tunnel was larger in the vertical direction than in the horizontal direction. The tensile strain and shear stress induced in the existing tunnel exceeded the cracking tensile strain and allowable shear stress limit given by the American Concrete Institute.

Keywords: perpendicularly crossing-tunnel interaction, three-dimensional centrifuge modeling, three-dimensional numerical analysis, effects of volume and weight losses

Introduction

When excavating a new tunnel closely beneath an existing tunnel, the existing tunnel may experience excessive induced stress and deformation. Some case studies have observed large differential tunnel settlement along with cracks on tunnel linings (Cooper et al., 2002; Mohamad et al., 2010; Li & Yuan, 2012). Thus, it is important to understand the interaction between two tunnels in order to assess potential ultimate and serviceability problems with an existing tunnel. However, the responses of an existing tunnel to the excavation of a new tunnel in the field are influenced by many factors that make data interpretation particularly difficult.

A limited number of studies related to tunnel responses to the excavation of a new tunnel have been conducted. Kim et al. (1998) carried out a series of tunnel-tunnel interaction tests using a 1-g model in clay. They found that the section of the existing tunnel directly above the new tunnel was vertically compressed due to the large jacking force induced by the installation of the liner of the new tunnel. Although tunnel responses to a new tunnel excavation have been investigated, the current understanding of how stress is redistributed on the existing tunnel is still limited. To improve this understanding, changes in stress on the existing tunnel should be studied.

The behavior of a pipeline beneath which a tunnel was excavated in sand has been investigated in centrifuge (Vorster et al., 2005; Marshall et al., 2010b). It was shown that soil-pipe stiffness has a significant influence on the longitudinal bending moment of a pipeline. Tunneling effects on a pipeline have also been investigated using an analytical solution, where elastoplastic soil-pipe-tunnel interaction was considered (Klar et al., 2007). In addition, numerical parametric studies have been carried out to investigate soil-pipe interaction with different focuses (Klar & Marshall, 2008; Lim et al., 2010; Marshall et al., 2010a; Wang et al., 2011; Shi et al., 2013).

The effects of ground loss (or volume loss) caused by tunneling are commonly simulated in a centrifuge test by fitting an annulus around a hollow mandrel to control a specified amount of water extracted (Marshall et al., 2012). Apart from the effects of volume loss, the effects of soil removal inside a tunnel (i.e., the effects of weight loss) also influence the shape and magnitude of ground surface settlement (Verruijt & Booker, 1996; Verruijt & Strack, 2008). When a tunnel is vertically compressed, additional ground surface settlement occurs above the centerline of the tunnel while heave occurs at some distance away according to the analytical solution suggested by Verruijt & Booker (1996). Using numerical analysis with an elastic soil model, Verruijt & Strack (2008) found that a net reduction in tunnel weight causes smaller and narrower ground surface settlement than if the tunnel weight is made equal to the weight of the removed soil. Thus, the effects of weight loss should be considered and simulated in a centrifuge test to improve the understanding of tunnel-tunnel interaction.

The major objective of this study was to investigate the responses of an existing tunnel to the excavation of a new tunnel underneath. Furthermore, the effects of volume and weight losses on the interaction between perpendicularly crossing tunnels were systematically studied in a centrifuge test. In this study, two three-dimensional centrifuge tests were carried out in a geotechnical centrifuge located at the Hong Kong University of Science & Technology (Ng et al., 2001, 2002). In addition, three-dimensional numerical back-analyses using a non-linear constitutive model with small strain stiffness were conducted to improve understanding of stress transfer on the existing tunnel.

Three-dimensional centrifuge modeling

Centrifuge model package

Figure 1a shows a typical plan view of the centrifuge model package of a new tunnel excavation perpendicularly underneath an existing tunnel. A soil model with the dimensions of approximately 1250 mm (*l*) x 930 mm (*w*) x 750 mm (*h*) was prepared for each test. A prototype stress condition can be created by applying a centrifugal acceleration using a geotechnical centrifuge. The gravitational acceleration used in this study was 60 times that of the earth. Appropriate centrifuge scaling laws are summarized in Table 1. A new model tunnel advanced in six excavation stages by 0.6D (where D is tunnel diameter) at a time underneath and at right angles to an existing model tunnel. Reference axes identifying tunnel orientation were defined. In particular the "X" axis and the "Y" axis referred to the longitudinal and transverse directions of the existing tunnel, respectively.

It was possible that the six-stage excavation of the new tunnel in this study did not lead to the plane strain conditions. Liu et al. (2009) reported a three-dimensional numerical analysis of a new tunnel excavation underneath and orthogonal to an existing tunnel in rock. They illustrated that the new tunnel excavation has a significant influence on the existing tunnel when the advancing tunnel face is within a distance of ±1D from the centerline of the existing tunnel. In the centrifuge model tests carried out in this study, the advancing tunnel face was located within a distance of ±1.5D from the centerline of the existing tunnel, which is larger than the distance of ±1D reported by Liu et al. (2009). Thus, it is believed that the six-stage tunnel excavation can adequately capture any significant changes in stress acting on the existing tunnel, even if plane strain conditions were not reached in the tests.

The two model tunnels had an outer diameter of 100 mm (equivalent to 6 m in prototype scale). The tunnel lining was made of aluminum alloy with a lining thickness equivalent to 180 mm in prototype scale. The thickness of the tunnel lining was converted to that of concrete with equivalent flexural stiffness. Young's modulus of concrete (E_c) was estimated to be 33 GPa by assuming that the compressive strength (f'_c) is 50 MPa (ACI, 2011). The tunnel lining thicknesses were thus equivalent to 230 and 420 mm in the transverse and longitudinal directions of each tunnel, respectively.

Figure 1b shows an elevation view of the centrifuge model package. Cover depth-to-diameter ratios (C/Ds) of the existing tunnel and the new tunnel were 2 and 3.5, respectively (i.e., cover depths were 12 and 21 m, respectively, in prototype scale). A pillar depth-to-diameter ratio (P/D) of 0.5 (i.e., the pillar depth was 3 m in prototype scale) was adopted, where the pillar depth is the clear distance between each tunnel. The instrumentation shown in the figure is explained in the following section. Toyoura sand was used due to its small particle size relative to the size of the model tunnels (i.e., the ratio of model tunnel size to particle size was 500). Thus, particle size effects were expected to be insignificant (Goodings and Gillette, 1996). The average particle size (D_{50}), maximum void ratio (e_{max}), minimum void ratio (e_{min}), specific gravity (G_s) and critical state internal friction angle (ϕ_c) of Toyoura sand are 0.17 mm, 0.977, 0.597, 2.64 and 30°, respectively (Ishihara, 1993). The sand sample was prepared in each test using a dry pluviation technique. The density of a soil sample was controlled by both the drop height of sand and the rate of pluviation, which in this study were 500 mm and about 100 kg per hour, respectively.

In-flight tunneling simulation technique

Figure 2a illustrates a novel modeling device, which is called the "donut", to simulate tunnel advancement in a centrifuge test. A pair of rubber bags, one mounted outside and the other mounted inside a model tunnel, was used to simulate the effects of both volume and weight losses at each stage of excavation in the centrifuge. The tunnel lining of 100 mm in diameter (or 6 m in prototype scale) was made of aluminum alloy and its lining bending stiffness per unit width of 0.16 kN.m^2/m (or 33.5 MN.m^2/m in prototype scale) and thickness of 3 mm (or 180 mm in prototype scale) were scaled properly.

During the centrifuge model preparation, each rubber bag was filled with a heavy fluid ($ZnCl_2$) having a density similar to that of the soil sample or about 1500 kg/m^3 to simulate the presence of soil. Each outer rubber bag was filled with a known amount of the heavy fluid representing an equivalent percentage of "volume loss", which in this study was 2%. Volume loss was simulated by controlling the outflow of the heavy fluid from the outer rubber bag. Likewise, each inner rubber bag was filled with the heavy fluid which was drained away at different stages to simulate weight loss due to tunnel excavation in the centrifuge.

Tunnel simulation in this study was intended to mimic the effects of closed-face shield tunneling. Mair & Taylor (1997) reported typical volume losses due to tunnel excavation using earth pressure balance shields in sand and soft clay of up to 1% and 2%, respectively. Shirlaw et al. (2003) and Abrams (2007) reported volume losses in mixed face tunneling involving clay and sand of between 1 and 4%. Based on these reports, a volume loss of 2% was adopted in this study.

Figure 2b shows the advancing sequence of the new model tunnel. Excavated sections 1 to 6 were assembled to form the new tunnel. Both ends of the new tunnel were closed to prevent the displacement of soil into the tunnel. The six advancing sections, each representing a length of 0.6D or 3.6 m in prototype scale, were controlled independently in-flight in a centrifuge test. Each rubber bag was connected to an outlet valve by a drainage tube. Each valve could be opened in-flight allowing outflow of the heavy fluid which was collected in a reservoir. To simulate effects of both volume and weight losses simultaneously, the two valves to which the inner and outer bags in each section were connected were regulated to simulate the effects of tunneling in-flight. To simulate only volume loss, only the valve to which the outer bag in each section was connected was regulated, whereas the valve to which the inner bag in the same section was connected was closed.

Test program

Two centrifuge tests were conducted. In Test S, the effects of volume and weight losses due to the excavation of a new tunnel were modeled simultaneously. In Test VW, the effects of volume loss were simulated first followed by the effects of weight loss. When only the effects of volume loss are interpreted, the first part of Test VW is called Test V. Compared with Tests V and VW, Test S better simulates tunnel advancement conditions in the field. Thus, responses of the existing tunnel were mainly investigated in Test S. A summary of the modeling sequences carried out in both tests is given in Table 2.

In order to compare measured results from both tests, the densities of sand in both tests were controlled within the same range using the dry pluviation technique discussed previously. The average dry densities of sand in Test S and Test VW were 1529 and 1531 kg/m^3, equivalent to relative densities of 64% and 65%, respectively.

Instrumentation

Figure 3a illustrates the types and locations of instruments installed on the existing tunnel to investigate responses of the existing tunnel in the longitudinal and transverse directions. The existing tunnel was considered to be wished-in-place as both ends of the model tunnel were closed to prevent soil movement into the tunnel.

In the longitudinal direction of the existing tunnel, tunnel settlement was measured using linear variable differential transformers (LVDTs) connected to extension rods, which were fixed along the crown of the existing tunnel. The extension rods were encased in hollow tubes to minimize friction with the surrounding soil. During the dry pluviation of sand, the extension rods were temporarily supported by a structural frame, which was removed after the sand sample reached the desired height of 750 mm. In Test S, LVDTs measuring ground surface and tunnel settlement were separately installed on each side of the centerline of the new tunnel. The main purpose of this LVDT arrangement was to identify a zone of influence of the new tunnel excavation on the existing tunnel. After completing Test S, the LVDTs were moved closer to the centerline of the new tunnel where significant ground surface and tunnel settlement occurs so that the responses could be observed in Test VW.

To measure strain in the longitudinal direction of the existing tunnel, 14 sets of strain gauges or longitudinal bending moment transducers were installed along the crown and invert of the existing tunnel. Full Wheatstone bridge semiconductor strain gauges having a gauge factor of 140 were used to compensate for temperature effects.

In the transverse direction of the existing tunnel, Figure 3b shows a sectional view of the existing tunnel at the location directly above the new tunnel. Tunnel deformation was measured using four potentiometers installed at the crown, at each springline and at the invert to record changes in the horizontal and vertical diameters of the existing tunnel. The potentiometers were mounted on a plate connected to a frame that was fixed to the lining of the existing tunnel (see Fig. 1b). A linear potentiometer is a variable resistor connected to three leads. The first two leads are connected to both ends of the resistor, so the resistance between them is fixed. The third lead is connected to a slider that travels along the resistor varying the resistance between itself and the other two connections. Changes in resistance in a linear potentiometer are linearly proportional to the distance travelled by the slider (Todd, 1975). In this study, the accuracy of a potentiometer was about ±1 mm in prototype scale, taking into account the fluctuation of data before the start of the new tunnel excavation.

In addition to measuring the deformation of the existing tunnel, eight sets of strain gauges were installed evenly at an interval of 45^{o} around the tunnel circumference to measure strain in the transverse direction. Full Wheatstone bridge foil strain gauges having a gauge factor of 2 were used instead of the semiconductor type simply because it was not possible to mount the latter inside the model tunnel.

Test procedure

After the centrifuge model package was prepared and all transducers calibrated in 1g, the model package was transferred to the centrifuge platform. The centrifuge was gradually spun up to a nominal gravitational acceleration of 60g. Before commencing new tunnel advancement, sufficient time was allowed to ensure that there was no further ground surface settlement. Data from all the transducers measured at the acceleration of 60g were taken as initial readings. Subsequently, in-flight tunnel advancement was carried out according to the corresponding modeling sequence (refer to Table 2). Sufficient time was provided to allow all the transducer readings had stabilized before each excavated section was advanced to the next stage. After completion of tunnel advancement, the centrifuge was spun down.

Three-dimensional numerical back-analysis

In addition to centrifuge testing, numerical back-analyses were carried out using the commercial finite element program ABAQUS (Hibbitt et al., 2008).

Finite element mesh and boundary conditions

Figure 4a shows the three-dimensional finite element mesh used to back-analyze the two tests. The mesh replicated the model geometry of the centrifuge test. Owing to symmetry, only half of the entire mesh was required. The mesh had dimensions of 625 mm x 930 mm x 750 mm in model scale. An eight-node brick element was used to model the soil. The boundaries adopted in the finite element analysis consisted of roller supports applied to three vertical sides (i.e., planes ABCD, BCGF and EFGH) and pin supports applied to the base of the mesh (i.e., plane CDHG). A plane of symmetry was identified and applied at X/D=0 (i.e., plane ADHE).

Apart from the back-analysis of centrifuge tests, a greenfield case (i.e., without the presence of the existing tunnel) was carried out using the same mesh to compare and highlight the difference between computed ground surface settlements due to the construction of the new tunnel with and without the presence of the existing tunnel.

Figure 4b shows details of the two perpendicularly crossing tunnels. A four-node shell element was used to model the tunnel lining. A tie constraint between the outer surface of the existing tunnel and the surrounding soil was adopted. For ease of identification and comparison, a monitoring section of the existing tunnel was located directly above the new tunnel (i.e., X/D = 0).

Constitutive model and model parameters

A hypoplastic constitutive model with small strain stiffness was adopted in this study to model dry Toyoura sand. Hypoplastic constitutive models were developed to describe the non-linear response of granular material (Kolymbas, 1991; Gudehus, 1996; von Wolffersdorff, 1996; Wu et al., 1996; Gudehus & Mašín, 2009; Mašín, 2012). Intergranular strain concept or small strain stiffness has been incorporated into hypoplastic constitutive models (Niemunis & Herle, 1997). Herle & Gudehus (1999) reported calibration results of model parameters (ϕ_c, h_s, n, e_{do}, e_{co} and e_{io}) for Toyoura sand. Triaxial test results of Maeda and Miura (1999) was used to determine exponent α and β by curve fitting. Small strain stiffness or intergranular strain concept parameters (m_R, m_T, R, β_r and χ) were calibrated by curve fitting the triaxial test results with local strain measurements of Yamashita et al. (2000).

The coefficient of at-rest earth pressure K_0 was assumed to be 0.5. The model parameters are summarized in Table 3.

The tunnel lining made of aluminum alloy was modeled as a linear elastic material with a Young's modulus of 69 GPa. Density and Poisson's ratio of the tunnel lining were assumed to be 2700 kg/m^3 and 0.33, respectively.

Numerical modeling procedures

The numerical modeling of the tunnel-tunnel interaction basically followed the centrifuge test procedure. Since centrifuge tests were carried out in dry sand, drained effective stress analysis was adopted in the numerical modeling. First, a gravitational acceleration of 60g was incrementally applied. The existing tunnel and the lining of the new tunnel were modeled as wished-in-place. To back-analyze the centrifuge model tests, the volume of heavy fluid, which has the same unit weight as the soil adopted, was modeled as being identical to the volume of soil elements around and inside the lining of the new tunnel. For simulating new tunnel advancement numerically, the soil elements that produced an equivalent volume loss of 2% were "removed" by deactivating the relevant soil elements around the lining of the new tunnel. Likewise, relevant soil elements inside the lining of the new tunnel were "excavated" or deactivated to mimic the effects of weight loss. Modeling sequences of tunnel advancement in numerical analysis were identical to those in centrifuge tests (refer to Table 2).

Interpretation of results

Measured and computed results reported in this study are in prototype scale unless otherwise stated. In order to assess any serviceability problem with the existing tunnel, both measured and computed results were compared with subway tunnel codes of practices (BTS, 2000; LTA, 2000; BD, 2009). In addition, measured field data from two case histories of crossing tunnels were obtained for comparisons. Details of the case histories are summarized in Table 4.

Surface settlement above the existing tunnel

Figure 5 compares measured and computed surface settlements normalized by tunnel diameter (δ/D) for different modeling sequences at the end of tunneling. The imposed volume loss was 2% in each test. In Test S, where the effects of volume and weight losses were modeled simultaneously, the measured maximum normalized surface settlement was about 0.34% (20 mm). When only the effects of volume loss were simulated (Test V), the maximum normalized surface settlement was about 15% larger than that in Test S. This is because soil heave due to weight loss (or stress relief) was not simulated in Test V, resulting in the larger ground surface settlement. On the other hand, when the effects of weight loss were simulated after the simulation of volume loss (Test VW), additional surface settlement was induced. The maximum surface settlement in Test VW was about 10% larger than that in Test V. This finding was somewhat unexpected initially, but after detailed investigation it was revealed that when the heavy fluid inside the rubber bags mounted inside the tunnel lining was drained away, the supporting pressure exerted by the heavy fluid on the new tunnel lining was removed. Consequently, the new tunnel was compressed vertically by overburden pressure (to be further discussed later) causing the additional surface settlement. Although the removal of soil from inside the new tunnel in Test VW led to stress relief and hence soil heave, the effects of vertical compression of the new tunnel on ground settlement were more pronounced. Verruijt & Booker (1996) investigated the effects of vertical compression of a tunnel on ground surface displacements by an analytical elastic solution and they reported that surface settlement occurs directly above the tunnel whereas heave takes place at some distance away. In the physical model tests carried out in this study, however, the vertical compression of the new tunnel only caused surface settlement but not heave. This is expected since soil is not elastic, as assumed in the analytical elastic solution.

Although the overall trends between measured and computed results were comparable, the maximum measured and computed surface settlements of Tests S, V and VW still differed by 30, 14 and 8 %, respectively. One of the possible reasons for the discrepancies is that the stress-induced anisotropy computed implicitly by the hypoplastic constitutive model could not describe the induced soil anisotropic responses in centrifuge tests exactly. Ng & Lee (2005) have illustrated that the magnitude and profile of computed ground surface settlements are strongly influenced by the degrees of stiffness anisotropy assumed in their numerical simulations.

To investigate the effects of the existing tunnel on the surface settlement induced by the advancing perpendicularly crossing tunnel underneath, computed results of the greenfield case were also compared with the computed surface settlements above the existing tunnel for the three cases (S, V and VW) considered. The computed greenfield maximum surface settlement was significantly larger than (about 65%) that due to the presence of the existing tunnel. Thus, stiffening effects due to the presence of an existing tunnel should not be ignored in design analysis.

Settlement of the existing tunnel and tunnel gradient

Figure 6 shows the measured and computed settlements of the existing tunnel in the longitudinal direction at the end of tunnel excavation. Maximum measured normalized tunnel settlement (δ/D) in Test S was about 0.3% (18 mm) which exceeded one allowable limit of 15 mm (LTA, 2000) but was still within another allowable limit of 20 mm (BD, 2009). Settlement of the existing tunnel for different modeling sequences had the same overall trend as the measured ground surface settlement above the existing tunnel (refer to Fig. 5). The tunnel settlement measured in Test V and Test VW were larger than those measured in Test S and exceeded the permissible limits set by LTA (2000) and BD (2009). The measured and computed tunnel settlements in Test S were comparable, suggesting that the stress transfer mechanism on the existing tunnel may be investigated using numerical analysis.

The gradient of the existing tunnel was calculated from the slope of measured settlement of the existing tunnel. The maximum tunnel gradient in Test S of 1:1600 exceeded one limit of 1:2500 (Li & Yuan, 2012) but was still within another limit of 1:1000 (LTA, 2000; BD, 2009). The maximum gradient was located at a distance of about 2.5D from the centerline of the new tunnel (i.e., X/D = 2.5).

In addition, settlements of the existing tunnel and gradients in Test S were compared with data from two case histories where the settlement of an existing tunnel was induced by a new tunnel excavation underneath. Given the potential differences between field monitoring and centrifuge tests in terms of ground conditions, tunneling methods and the flexural rigidity of the tunnel (see Table 4), the field monitoring data and centrifuge test results cannot be compared quantitatively but it is possible to illustrate qualitatively the general trend of settlement of the existing tunnel.

Induced strain and shear stress in the longitudinal direction of the existing tunnel

Figure 7 illustrates the induced strains measured along the invert in the longitudinal direction of the existing tunnel at the end of tunnel excavation. Induced strain in the longitudinal direction of the existing tunnel was measured by strain gauges installed at the crown and the invert of the existing tunnel (refer to Fig. 3a). Due to the new tunnel excavation, sagging moment was induced at the location directly above the new tunnel (i.e., X/D = 0), resulting in tensile (+ve) and compressive (-ve) strain induced at the invert and the crown of the existing tunnel, respectively. The cracking tensile strain of unreinforced concrete is 150 με (ACI, 2001). In Test S, the maximum tensile strain of about 152 με was induced at the location directly above the new tunnel. Hence cracks might appear on the lining of the existing tunnel. Although most of the tunnel lining was made of reinforced concrete, induced tensile strain can widen the gap in the circumferential joint and cause water leakage. The maximum induced tensile strain was larger in Tests V and VW than in Test S within a distance of 2D from the centerline of the new tunnel (i.e., from X/D = 0 to 2). This is because the maximum settlement of the existing tunnel was larger in Tests V and VW than in Test S (refer to Fig. 6).

The shear stress on the tunnel lining was deduced from the slope of the induced strain in the longitudinal direction of the existing tunnel. For comparison purposes, an allowable shear stress of 660 kPa was estimated according to an assumed concrete compressive strength (f'_c) of 50 MPa and a reduction factor of 0.55 (ACI, 2011). In Test S, the maximum shear stress was 780 kPa, which exceeded the allowable shear stress, suggesting that cracks might have appeared on the tunnel lining. There was large shear stress on the lining of the existing tunnel at a distance between 2D and 3D from the centerline of the new tunnel.

Liu (1990; cited by Liao et al., 2008, p. 428) reported a case history from Shanghai in which diagonal cracks were observed on tunnel linings when differential settlement occurred on a water transmission tunnel. Liao et al. (2008) suggested that shear stress in the tunnel lining was one of the key factors influencing tunnel deformation. The cracks in their study were located in an area between the location of maximum tunnel settlement and the inflection point of the tunnel. In this study, the inflection point was estimated to be at a distance between 2.5D and 3D from the centerline of the new tunnel.

Given the effects of volume and weight losses on cross-tunnel interaction were investigated separately, it is evident that the trends of surface and tunnel settlements and induced strains in the longitudinal direction of the existing tunnel in the two tests are all similar but differ only in magnitude. Thus, it suffices to report results from Test S only from now on.

Tunnel deformation

Figure 8a shows measured and computed deformations of the existing tunnel (at X/D = 0) during the advancement of the new tunnel in Test S. It can be seen that the existing tunnel was vertically compressed and horizontally elongated as the new tunnel advanced. The measured maximum normalized vertical compression and horizontal elongation of the existing tunnel were 0.04% and of 0.07%, respectively. The measured maximum normalized vertical compression and horizontal elongation of the existing tunnel occurred when the new tunnel face was at -0.3D and -0.9D away from the centerline of the existing tunnel, respectively. When the excavated section of the new tunnel was directly underneath the existing tunnel (i.e., at Y/D = 0.3), a significant reduction in both vertical compression and horizontal elongation of the existing tunnel was observed. As the new tunnel passed the existing tunnel, the existing tunnel continued to deform but at a reduced rate.

On the other hand, the computed results show almost the same magnitude (or symmetrical) of vertical compression and horizontal elongation of the existing tunnel due to the advancement of the new tunnel. This is because uniform soil displacement around the new tunnel was imposed in the numerical analysis. In the centrifuge test, however, soil displacement around the new tunnel was unlikely to be uniform, resulting in the unsymmetrical measured vertical compression and horizontal elongation of the existing tunnel. The computed maximum vertical compression of the existing tunnel is about two times larger than the measured one when the advancing tunnel face was located at less than half the tunnel diameter (i.e., at Y/D = -0.3) away from the centerline of the existing tunnel. The maximum horizontal elongation is similarly over-predicted at Y/D = -0.3. However, both measured and computed results suggest that the most critical vertical compression and horizontal elongation of the existing tunnel occurred when the approaching new tunnel face was between -0.9D and -0.3D away from the existing one. At the end of new tunnel excavation, measured and computed deformations of the existing tunnel were consistent with each other. This increase the confidence in the conclusions derived from the test.

According to one code of practice (BTS, 2000), the minimum and maximum diameters of a tunnel should not differ by more than 2% (i.e., $(D_{max} - D_{min})/D_0 \leq 2\%$), where D_0 is the initial diameter of the tunnel which equals to 6 m in this study. This allowable limit was not exceeded. But because the existing tunnel was vertically compressed even before the new tunnel excavation due to the vertical stress being larger than the horizontal stress (i.e., $K_0 < 1$), induced deformation may enlarge the gap in the radial joint and cause water leakage.

Kim et al. (1998) carried out a 1-g physical model test of crossing tunnels in clay. They reported that the existing tunnel was compressed vertically by the large jacking forces from the miniature tunneling machine when the new tunnel liner was driven. The lining of the new tunnel in this study was wished-in-place before tunnel excavation. As the new tunnel advanced, the existing tunnel was compressed vertically. This is because stress transfer due to the new tunnel excavation caused an increase in the vertical stress acting on the existing tunnel. More explanations are given later.

Figure 8b shows the computed deformation of the new tunnel at the location directly underneath the existing tunnel (i.e., Y/D = 0) to explain the effects of different modeling sequences on ground surface settlement (Fig. 5) and settlement of the existing tunnel (Fig. 6). In case S, the tunnel was slightly vertically compressed due to the vertical stress being larger than the horizontal stress when K_0 was smaller than 1. On the contrary, when the soil around the new tunnel was removed but not the soil inside the tunnel in case V, the tunnel became elongated vertically. This is because the vertical stress of soil inside the new tunnel was larger than the horizontal stress. However, after the soil inside the new tunnel was removed (case VW), which effectively meant that the supporting pressure inside the tunnel was also removed causing additional ground settlement above the new tunnel, the new tunnel became vertically compressed. The vertical compression of the new tunnel at the end of excavation was about three times larger in case VW than in case S. Consequently, in case VW the vertical compression of the new tunnel dominated the effects of stress relief due to soil removal from inside the new tunnel.

Induced strain in the transverse direction of the existing tunnel

Figure 9 shows the measured and computed strains induced at the outer face of the existing tunnel at the end of tunnel excavation in Test S. Induced strains at the outer face of the existing tunnel were measured by strain gauges fixed to the tunnel lining in the transverse direction at the location directly above the new tunnel (refer to Fig. 3b). The positive and negative signs denote induced tensile and induced compressive strain, respectively. According to the measured results, there was induced compressive strain at the crown, shoulders, knees and invert while there was induced tensile strain at both springlines. By considering strain in the transverse direction, it was confirmed that the existing tunnel was vertically compressed and horizontally elongated (see Fig. 8a). Computed results were comparable to measured results, suggesting that the tunnel responses and stress transfer mechanism in the transverse direction of an existing tunnel may be studied using numerical analysis.

From measured results, the maximum induced compressive strain and induced tensile strain of 67 and 56 $\mu\varepsilon$ occurred at the invert and at the left springline, respectively. The maximum tensile strain on the tunnel lining was still below the cracking tensile strain limit of 150 $\mu\varepsilon$ (ACI, 2001). However, if strain in the transverse direction was large even before the start of the new tunnel excavation, tunneling may cause cracks on the lining of the existing tunnel. It should be noted that induced strain was more significant in the vertical and horizontal directions (i.e., at the crown, springlines and invert) than in the diagonal direction (i.e., at the shoulders and knees). However, this observation may only be applicable for the soil type and in-situ stress conditions adopted in this study.

Incremental normal stress on the existing tunnel

Figure 10a shows the computed incremental normal stress in the transverse direction of the section of the existing tunnel directly above the new tunnel in case S. The effects of the changes in normal stress on the responses of the existing tunnel in the transverse direction were investigated at four chosen locations—the crown, both springlines and the invert. The positive and negative signs denote increases and decreases in stress relative to that before tunneling, respectively. At the crown, normal stress increased as a result of stress transfer in the longitudinal direction of the new tunnel (Ng & Lee, 2005). At both springlines, normal stress reduced slightly. At the invert, there was a sharp reduction of normal stress when the excavated section of the new tunnel reached directly underneath the existing tunnel (i.e., Y/D = 0.3).

To investigate tunnel deformations, net incremental stress is adopted and defined as the difference between the summation of stresses in the vertical direction and the summation of stresses in the horizontal direction acting on the existing tunnel ($[\Delta\sigma_{Cr}+\Delta\sigma_{In}] - [\Delta\sigma_{L\text{-}sp}+\Delta\sigma_{R\text{-}sp}]$). The positive and negative signs of computed net incremental stress denote an increase and a decrease in stress in the vertical direction on the existing tunnel, respectively. When the new tunnel advanced towards the existing tunnel (i.e., from Y/D = -1.5 to -0.3), there was an increase in net incremental stress suggesting that the existing tunnel was vertically compressed. On the other hand, when the new tunnel advanced beyond the existing tunnel (i.e., from Y/D = 0.3 to 1.5), a reduction in net incremental stress occurred, suggesting that the existing tunnel was elongated vertically. At the end of new tunnel excavation, the computed net incremental stress approached zero, revealing there was little change in the diameter of the existing tunnel. This is consistent with the measured and computed deformation of the existing tunnel shown in Figure 8a.

Figure 10b illustrates the computed normal stress distribution along the crown and invert in the longitudinal direction of the existing tunnel at the end of excavation in Test S. At the location directly above the new tunnel (i.e., from X/D = 0 to 0.5), stress increased substantially at the crown whereas it decreased significantly at the invert of the existing tunnel. Along the crown, normal stress decreased as the distance away from the centerline of the new tunnel increased. On the other hand, normal stress along the invert increased with distance until it reached a peak at 2D away from the new tunnel's centerline.

The large tunnel settlement (Fig. 6), large induced strain in the longitudinal direction and large shear stress (Fig. 7) are mainly caused by two factors. First, soil arching caused a sharp reduction in vertical stress above the centerline of the new tunnel and an increase in vertical stress at some distance away due to stress redistribution along the invert of the existing tunnel. Second, overburden stress transfer along the crown of the existing tunnel caused vertical stress to increase substantially. Soil arching is explained in the next section.

The changes in normal stress acting on both the crown and the invert of the existing tunnel exceeded the limits defined in two codes of practice (i.e., +15 kPa for LTA, 2000; ±20 kPa for BD, 2009). Up to an offset distance of 1.5D from the centerline of the new tunnel, changes in normal stress along the crown of the existing tunnel also exceeded the allowable limit. Along the invert, normal stress reduced by more than the codes of practice would allow in the area between the centerline and a distance of 1D away from the centerline of the new tunnel. At a distance of 1.5D to 5D away from the centerline of the new tunnel, the increase in normal stress along the invert exceeded the recommended limits as well. Thus, the structural capacity of the existing tunnel should be reviewed based on changes in the loading condition around it.

Direction of principal stress

Figures 11a and 11b show the computed directions of principal stress in case S in the transverse direction of the existing tunnel before tunnel excavation and when the new tunnel reached the fourth section (Ex4 in the figures), respectively. There was a slight decrease in the magnitude of principal stress above each of section 1 to 3 (Ex1 to Ex3) as a result of tunnel excavation in each previous stage. Directly underneath the invert of the existing tunnel (i.e., above Ex4), both minor and major principal stresses reduced sharply. They did so because the soil above the existing tunnel tended to settle due to the new tunnel excavation but was prevented from doing so by the existing tunnel. Subsequently, overburden stress was transferred to the crown of the existing tunnel as a result of stress redistribution in the longitudinal direction of the new tunnel causing an increase in the major principal stress. The stress transfer around the existing tunnel resulted in a decrease in normal stress at the invert and both springlines and an increase in normal stress at the tunnel crown when the section of the new tunnel directly underneath the existing tunnel was being excavated (refer to Fig. 10a; when Y/D = 0.3).

Figures 11c and 11d show the computed directions and magnitudes of principal stresses in the longitudinal direction of the existing tunnel, before tunnel advancement and after the new tunnel reached the fourth section (Ex4), respectively. As expected, the magnitudes (i.e., sizes of vectors) of both major and minor principal stresses near the new tunnel reduced substantially due to the effects of volume loss (or shearing) and stress relief, which in turn were due to the advancement of the new tunnel. As illustrated by the rotation of principal stresses, shear stress was induced due to the excavation of the new tunnel. Since the existing tunnel and the soil further away from the new tunnel (i.e., that directly above Ex5 and Ex6 in Fig. 11b and at X/D greater than 1 in Fig. 11d) should have larger shear strength and stiffness than the soil closer to the new tunnel due to stress relief and shearing, stress redistribution (or soil arching) took place to maintain the overall equilibrium, as revealed by the rotations and the increases in magnitude of principal stresses of the soil above the existing tunnel in Figures 11b and 11d. Also soil arching caused principal stress to rotate in direction in the soil located at X/D greater than 1 and below the invert of the existing tunnel (see Fig. 11d).

Summary and conclusions

Three-dimensional centrifuge and numerical investigations of the interaction between two perpendicularly crossing tunnels were carried out in dry sand. In order to simulate the effects of both volume and weight losses on an existing tunnel due to the construction of a new tunnel underneath, a novel "donut" was developed to control volume loss and to mimic soil removal in-flight. Based on the measured and computed results, the following conclusions may be drawn:

1. The measured maximum ground surface settlement was the smallest when the effects of both volume and weight losses were modeled simultaneously (i.e., Test S). On the other hand, the surface settlement induced when the effects of weight loss were simulated after modeling volume loss (i.e., Test VW) was 10% larger than that induced when only volume loss was simulated (i.e., Test V). This is

because when the heavy fluid inside the rubber bags mounted inside the tunnel lining was drained away, the supporting pressure exerted by the heavy fluid on the lining of the new tunnel was removed. Consequently, the new tunnel was compressed vertically by overburden pressure, causing the additional surface settlement. Numerical simulations show that the presence of an existing tunnel can stiffen the ground and reduce ground surface settlement due to new tunnel excavation significantly.

2. The measured settlement of the existing tunnel was 15% larger in Test V than that in Test S. This is because the removal of soil mass in Test S led to stress relief resulting in ground heave which reduced the settlement induced by volume loss. However, there was about 10% more tunnel settlement in Test VW than in Test V. This is because the removal of soil from inside the new tunnel resulted in a reduction in supporting pressure on the tunnel lining, leading to the vertical compression of the new tunnel. This in turn induced settlement of the existing tunnel above it. The measured ground surface settlements were consistent with the observed tunnel settlements in all tests.
3. Due to the excavation of a new tunnel underneath the existing tunnel, the maximum measured settlement of the existing tunnel in Test S was 0.3%D, where D is tunnel diameter. This settlement exceeded the permissible limits of serviceability (e.g. LTA, 2000). Moreover, the measured tensile strain and shear stress induced in the existing tunnel exceeded the cracking tensile strain (ACI, 2001) and allowable shear stress limit (ACI, 2011), respectively.
4. The section of the existing tunnel immediately above the new tunnel was vertically compressed at every stage of excavation of the new tunnel in Test S. This is

because net incremental normal stress on the existing tunnel was larger in the vertical direction than in the horizontal direction.

5. At the end of the tunnel excavation, computed vertical stress increased substantially at the crown of the existing tunnel located directly above the new tunnel. This is because of stress transfer in the longitudinal direction of the new tunnel during the tunnel advancement. On the other hand, there was a sharp reduction in the computed vertical stress at the invert of the section of the existing tunnel immediately above the new tunnel. As a result of soil arching and stress redistribution, however, the computed vertical stress acting on the invert of the existing tunnel increased significantly to reach a peak at an offset distance of about 2D from the centerline of the new tunnel.

Acknowledgements

The authors would like to acknowledge financial support from the Research Grants Council of the HKSAR (General Research Fund project 617410).

References

Abrams, A. J. (2007). Earth pressure balance (EPB) tunneling induced settlements in the Tren Urbano Project, Rio Piedras, Puerto Rico. Thesis (M. Eng.), Dept. of Civil and Environmental Engineering, Massachusetts Institute of Technology.

American Concrete Institute. (2001). Control of Cracking in Concrete Structures (ACI 224R-01). M.I.

American Concrete Institute. (2011). Building Code Requirements for Structural Concrete and Commentary (ACI 318M-11). M.I.

British Tunnelling Society (2000). Specification for Tunnelling. Thomas Telford, London.

Building Department (2009). Practice Note for Authorized Persons APP-24. Technical notes for guidance in assessing the effects of civil engineering construction / building development on railway structures and operations. Building department of the government of HKSAR.

Cooper, M. L., Chapman, D. N., Rogers, C. D. F. & Chan, A. H. C. (2002). Movements in the Piccadilly Line tunnels due to the Heathrow Express construction. Géotechnique 52(4): 243-257.

Goodings, D. J. & Gillette, D. R. (1996). Model size effects in centrifuge models of granular slope instability. Geotech. Testing J. 19(3): 277-285.

Gudehus, G. (1996). A comprehensive constitutive equation for granular materials. Soils and foundations 36(1): 1-12.

Gudehus, G. & Mašín, D. (2009). Graphical representation of constitutive equations. Géotechnique 59(2): 147–151.

Herle, I. & Gudehus, G. (1999). Determination of parameters of a hypoplastic constitutive model from properties of grain assemblies. Mechanics of cohesive-frictional materials 4: 461-486.

Hibbitt, Karlson & Sorensen Inc. (2008). ABAQUS theory manual, v 6.8. Hibbitt, Karlson & Sorensen Inc. R.I.

Hight, D. W., Gasparre, A., Nishimura, S., Minh, N. A., Jardine, R. J. & Coop, M. R. (2007). Characteristics of the London Clay from the Terminal 5 site at Heathrow Airport. Géotechnique 57(1): 3–18.

Ishihara K. (1993). Liquefaction and flow failure during earthquakes. Géotechnique 43(3): 351-415.

Kim, S. H., Burd, H. J. & Milligan, G. W. E. (1998). Model testing of closely spaced tunnels in clay. Géotechnique 48(3): 375-388.

Klar, A., Vorster, T. E. B., Soga, K., & Mair, R. J. (2007). Elastoplastic solution for soil-pipe-tunnel interaction. J. Geotech. Geoenviron. Engng. 133(7): 782–792.

Klar, A., & Marshall, A. M. (2008). Shell versus beam representation of pipes in the evaluation of tunneling effects on pipelines. Tunn. Undergr. Sp. Technol. 23(4): 431–437.

Kolymbas, D. (1991) An outline of hypoplasticity, Archive of Applied Mechanics 61: 143-151.

Land Transport Authority (2000). Code of practice for railway protection. Development & Building Control Department, Land Transport Authority, Singapore.

Li, X. G. & Yuan, D. J. (2012). Responses of a double-decked metro tunnel to shield driving of twin closely under-crossing tunnels. Tunn. Undergr. Sp. Technol. 28: 18–30.

Liao, S. M., Peng, F. L. & Shen, S. L. (2008). Analysis of shearing effect on tunnel induced by load transfer along longitudinal direction. Tunn. Undergr. Sp. Technol. 23: 421–430.

Lim, K. S.G., Hong, C. Y., Wang, Y. & Ng, C. W.W. (2010). Soil-structure interaction of tunnel excavation beneath existing buried pipeline. The 4th International Conference on Geotechnical Engineering and Soil Mechanics, November 2-3, 2010, Tehran, Paper No. 587.

Liu, J. H. (1990). Construction technical manual for municipal underground engineering in soft ground. Shanghai (in Chinese).

Liu, H. Y., Small, J. C. & Carter, J. P. & Williams, D. J. (2009). Effects of tunnelling on existing support systems of perpendicularly crossing tunnels. Computers and Geotechnics 36: 880–894.

Maeda, K. & Miura, K. (1999). Relative density dependency of mechanical properties of sands. Soils and Foundations 39(1): 69-79.

Mair, R. J. & Taylor, R. N. (1997). Theme lecture: Bored tunnelling in the urban environment. Proc. 14th International Conference in Soil Mechanics and Foundation Engineering, Hamburg, Balkema, pp. 2353-2385.

Marshall, A. M., Elkayam, I., & Klar, A. (2010a). Centrifuge and discrete element modelling of tunnelling effects on pipelines. 7th International Conference on Physical Modelling in Geotechnics 2010 (ICPMG 2010) (pp. 633–637). Zurich, Switzerland: A.A. Balkema Publishers.

Marshall, A. M., Klar, A., & Mair, R. J. (2010b). Tunneling beneath buried pipes: view of soil strain and its effect on pipeline behavior. J. Geotech. Geoenviron. Engng. 136(12): 1664–1672.

Marshall, A. M., Farrell, R., Klar, A. & Mair, R. (2012). Tunnel in sands: the effect of size, depth and volume loss on greenfield displacements. Géotechnique 62(5): 385-399.

Mašín, D. (2012). Hypoplastic Cam-clay model. Géotechnique 62(6): 549–553.

Mohamad, H., Bennett, P. J., Soga K., Mair R. J. & Bowers, K. (2010). Behaviour of an old masonry tunnel due to tunnelling-induced ground settlement. Géotechnique 60(12): 927–938.

Ng, C. W. W., Van Laak, P. Tang, W. H., Li, X. S. & Zhang, L. M. (2001). The Hong Kong Geotechnical Centrifuge. Proc. 3rd Int. Conf. Soft Soil Engineering, Dec., Hong Kong. pp. 225-230.

Ng, C. W. W., Van Laak, P. A., Zhang, L. M., Tang, W. H., Zong, G. H., Wang, Z. L., Xu, G. M. & Liu, S. H. (2002). Development of a four-axis robotic manipulator for centrifuge modeling at HKUST. Proc. Int. Conf. on Physical Modelling in Geotechnics, St. John's Newfoundland, Canada, pp. 71-76.

Ng, C. W. W. & Lee, G. K. T. (2005). Three-dimensional ground settlements and stress transfer mechanisms due to open-face tunnelling. Can. Geotech. J. 42: 1015–1029.

Niemunis, A. & Herle, I. (1997). Hypoplastic model for cohesionless soils with elastic strain range. Mechanics of cohesive-frictional materials 2: 279-299.

Shi, J. W., Wang, Y., & Ng, C. W. W. (2013). Buried pipeline responses to ground displacements induced by adjacent static pipe bursting. Can. Geotech. J. 50(5): 481-492.

Shirlaw, J. N., Ong, J. C. W., Rosser, H. B., Tan, C. G., Osborne, N. H. & Heslop, P. E. (2003). Local settlements and sinkholes due to EPB tunnelling. Geotechnical Engineering 156 (GE4): 193–211.

Taylor, R. N. (1995). Geotechnical Centrifuge Technology. Blackie Academic and Professional, London.

Todd, C. D. (1975). The potentiometer handbook. McGraw-Hill, New York.

Verruijt, A. & Booker, J. R. (1996). Surface settlements due to deformation of a tunnel in an elastic half plane. Géotechnique 46(4): 753-756.

Verruijt, A. & Strack, O. E. (2008). Buoyancy of tunnels in soft soils. Géotechnique 58(6): 513–515.

Viana da Fonseca, A., Matos Fernandes, M. & Silva Cardoso, A. (1997). Interpretation of a footing load test on a saprolitic soil from granite. Géotechnique 47(3): 633-651.

von Wolffersdorff, P. A. (1996). A hypoplastic relation for granular materials with a predefined limit state surface. Mechanics of cohesive-frictional materials 1: 251-271.

Vorster, T. E. B., Klar, A., Soga, K. & Mair, R. J. (2005). Estimating the effects of tunneling on existing pipelines. J. Geotech. Geoenviron. Engng. 131(11): 1399-1410.

Wang, Y., Shi, J. W. & Ng, C. W. W. (2011). Numerical modeling of tunneling effect on buried pipelines. Can. Geotech. J. 48(7): 1125-1137.

Wu, W., Bauer, E. & Kolymbas, D. (1996). Hypoplastic constitutive model with critical state for granular materials. Mechanics of materials 23: 45-69.

Yamashita, S., Jamiolkowski, M. & Lo Presti, D.C.F. (2000). Stiffness nonlinearity of three sands. J. Geotech. Geoenviron. Engng. 126(10): 929-938.

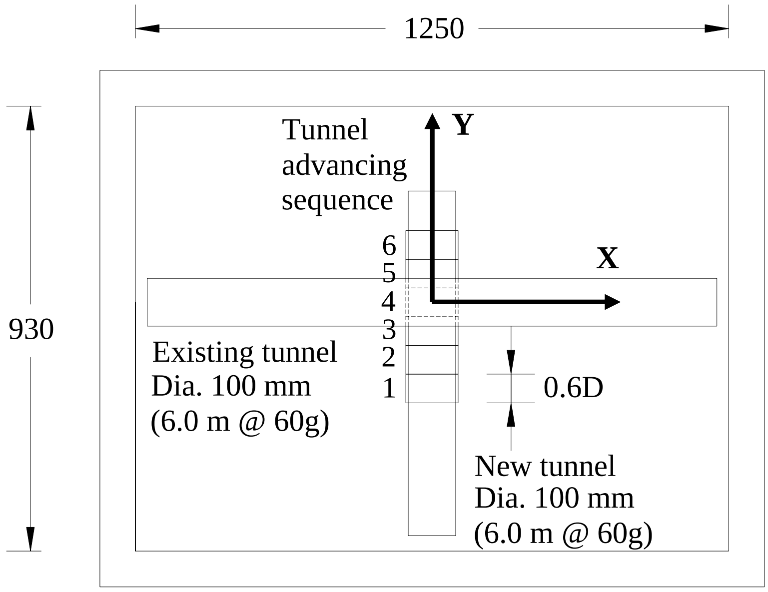

(a)

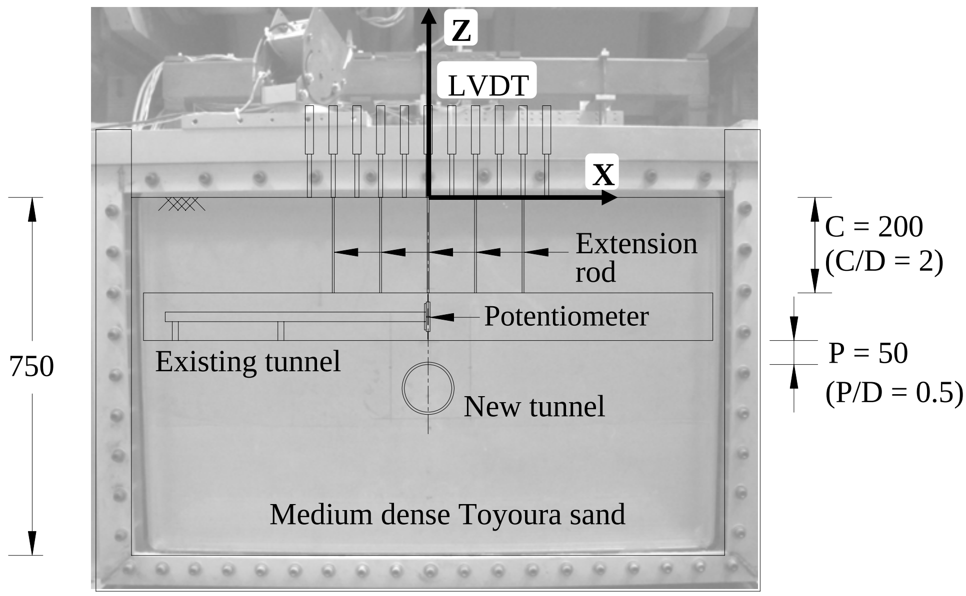

(b)

Note: Dimension in mm (model scale)

Figure 1 Schematic diagrams showing a centrifuge model package for simulating the interaction between perpendicularly crossing tunnels: (a) plan view; (b) elevation view

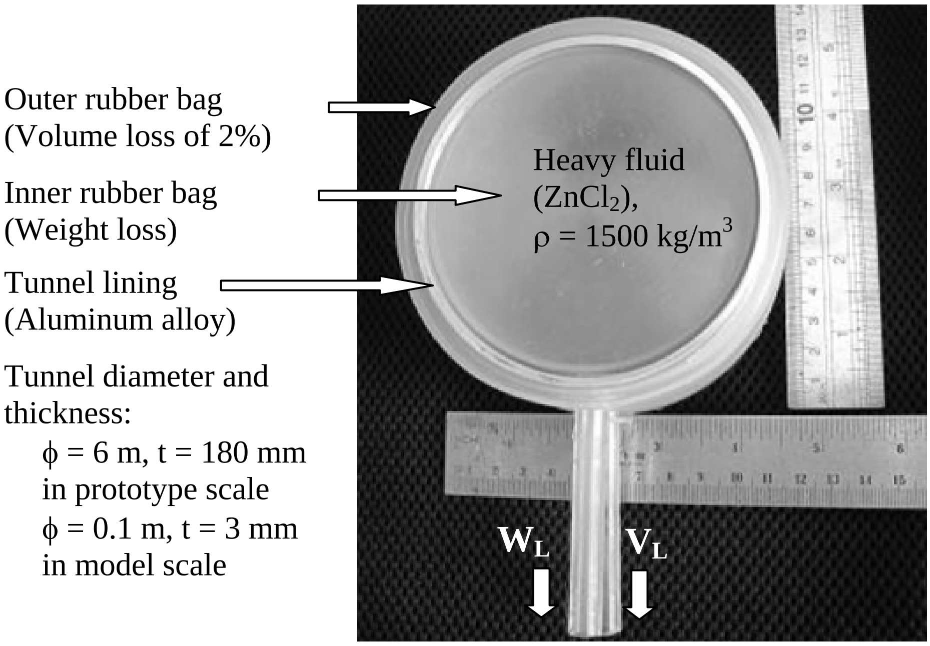

(a)

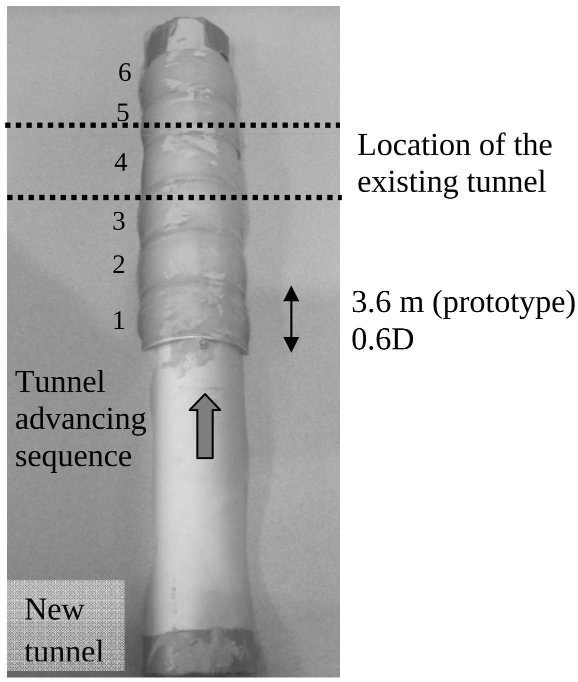

(b)

Figure 2 (a) The newly developed "donut" for simulating volume and weight losses simultaneously during tunnel advancement; (b) tunnel advancing sequence in a centrifuge test

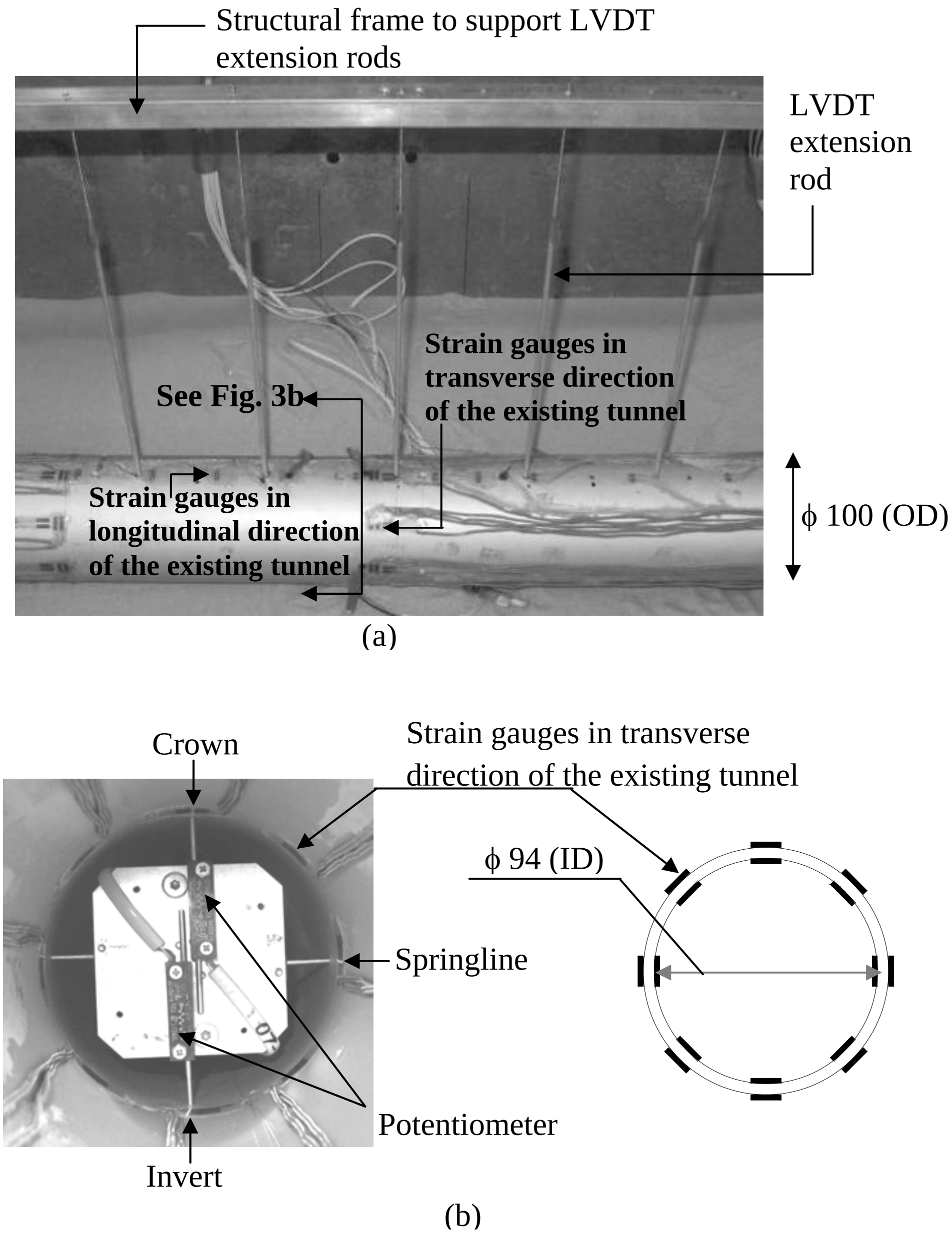

Note: Dimension in mm (model scale)

Figure 3 (a) Types and locations of instruments installed on the existing tunnel; (b) sectional view at mid-section of the existing tunnel showing arrangement of strain gauges and potentiometers

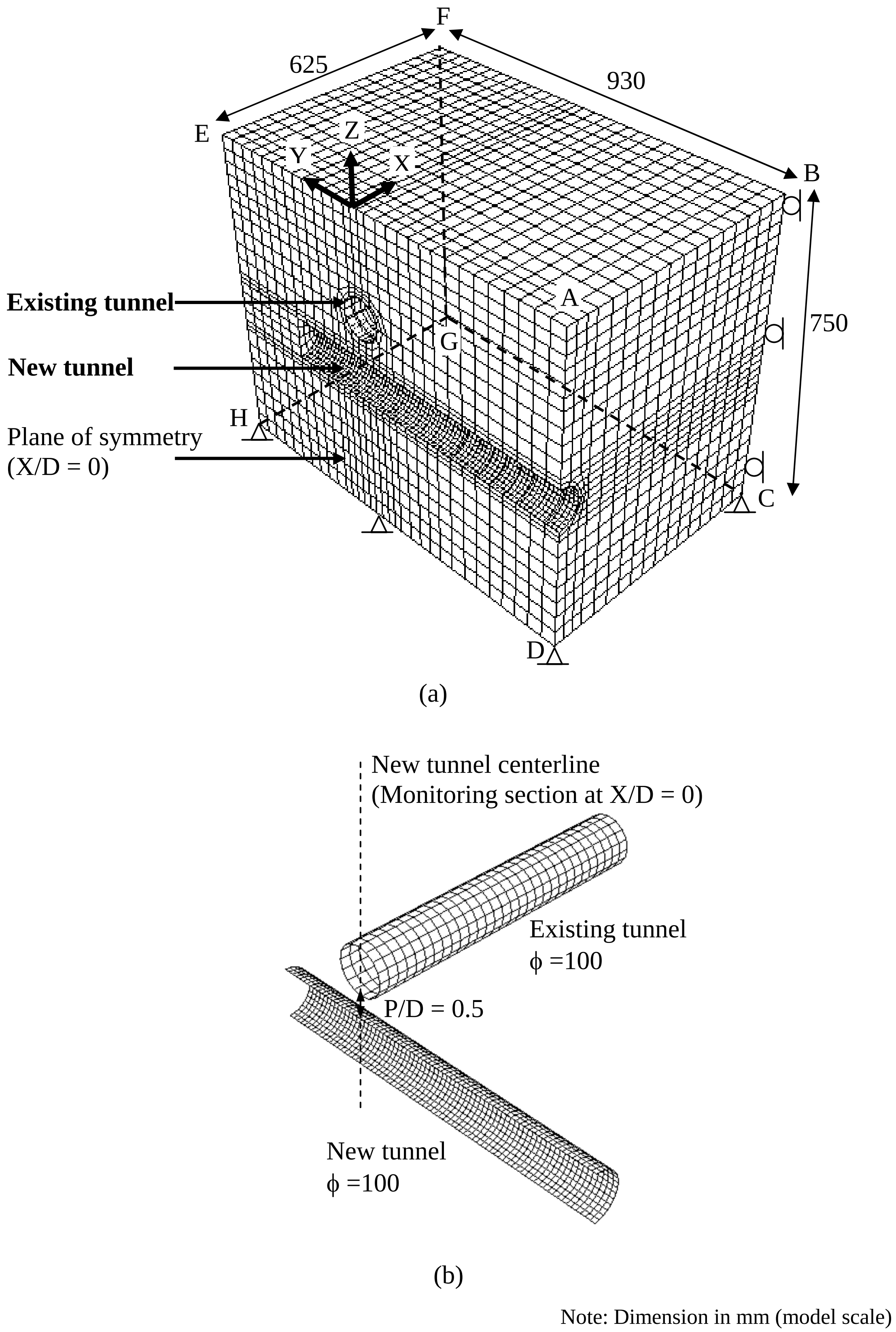

Figure 4 (a) The three-dimensional finite element mesh; (b) details of perpendicularly crossing tunnels

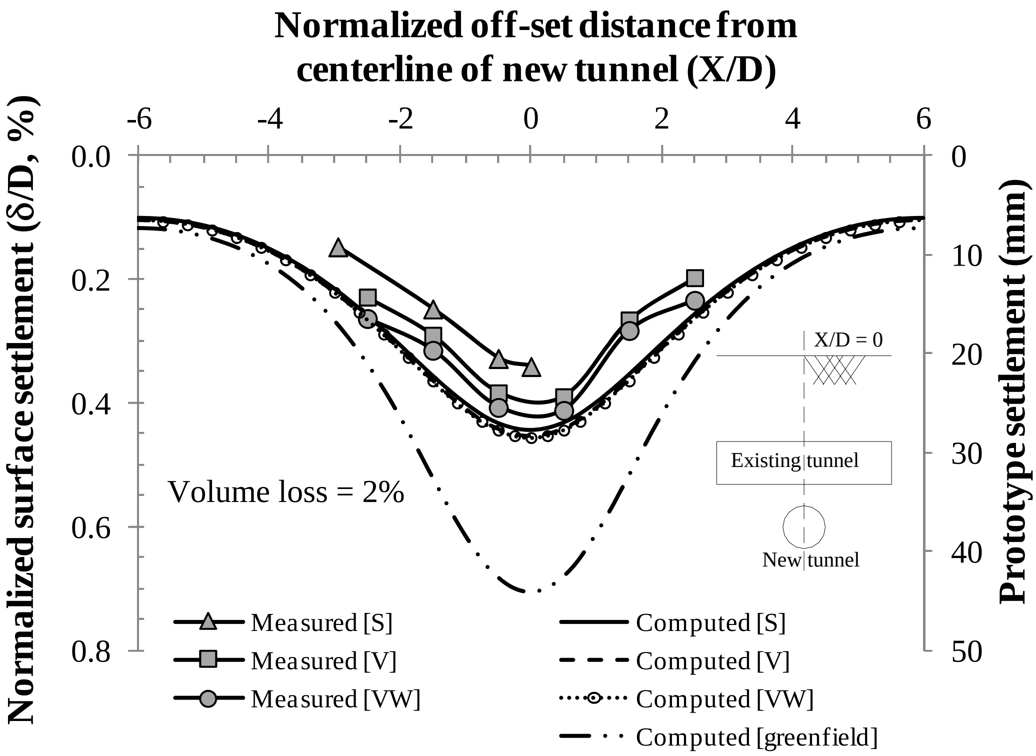

Figure 5 Comparison of measured and computed surface settlement

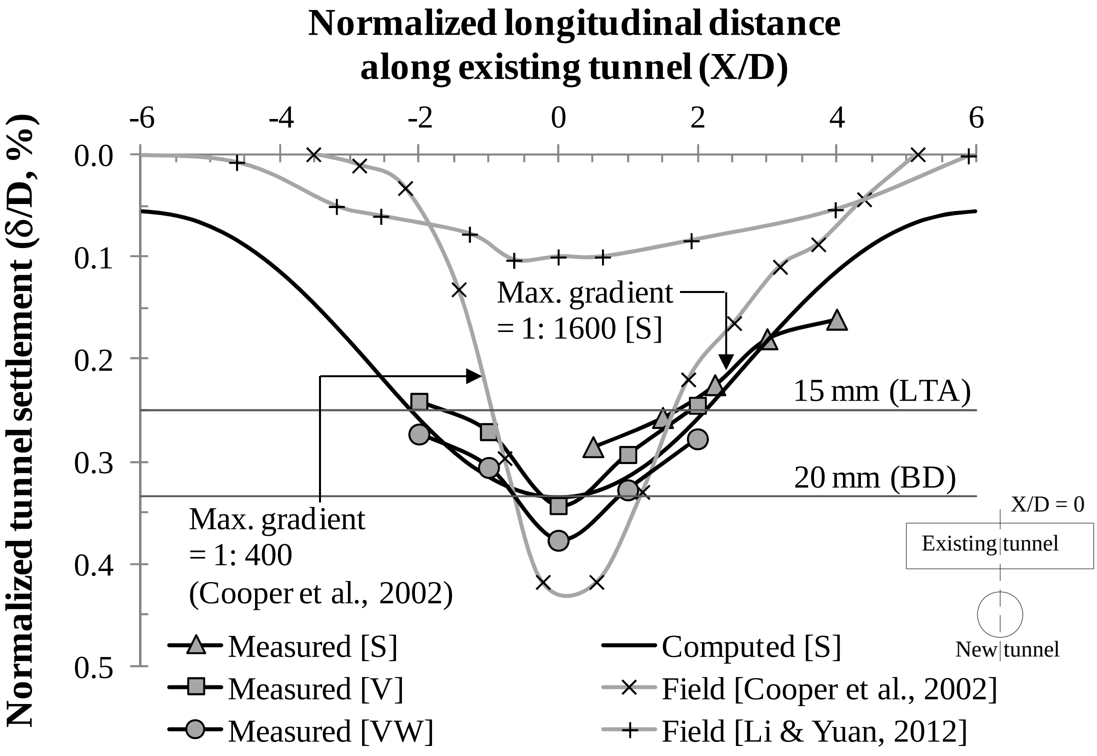

Figure 6 Comparison of measured and computed settlement of the existing tunnel

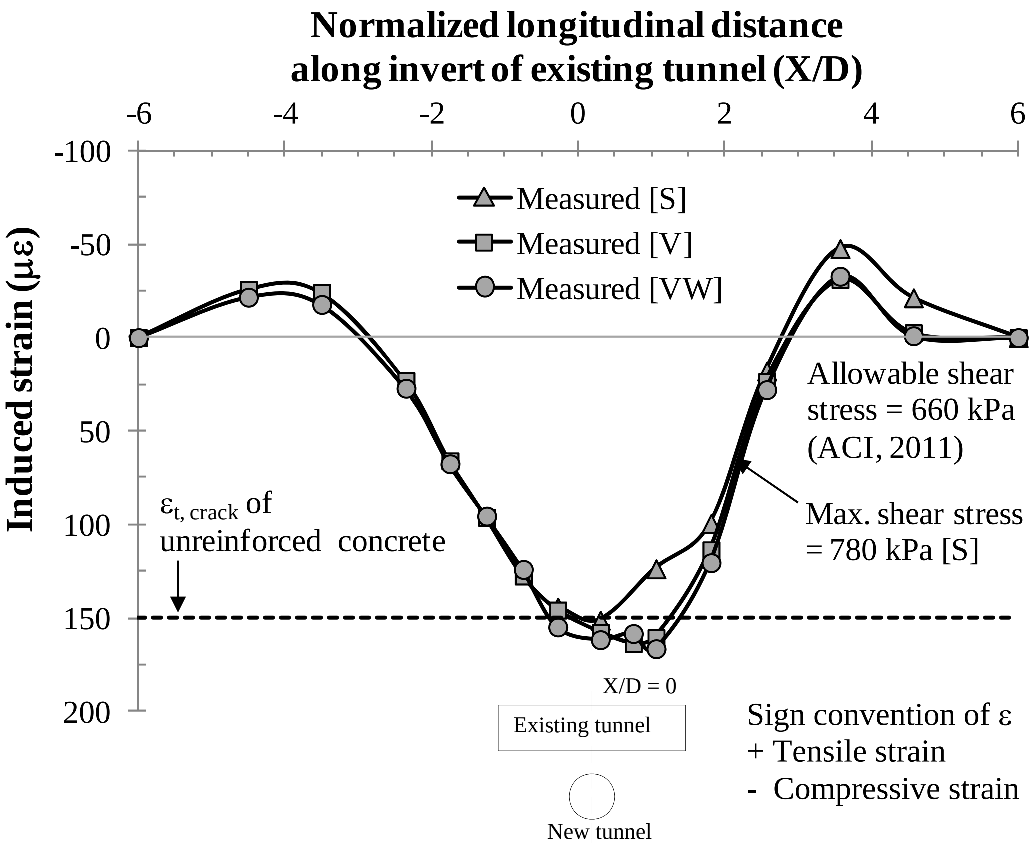

Figure 7 Induced strain measured along the invert in the longitudinal direction of the existing tunnel

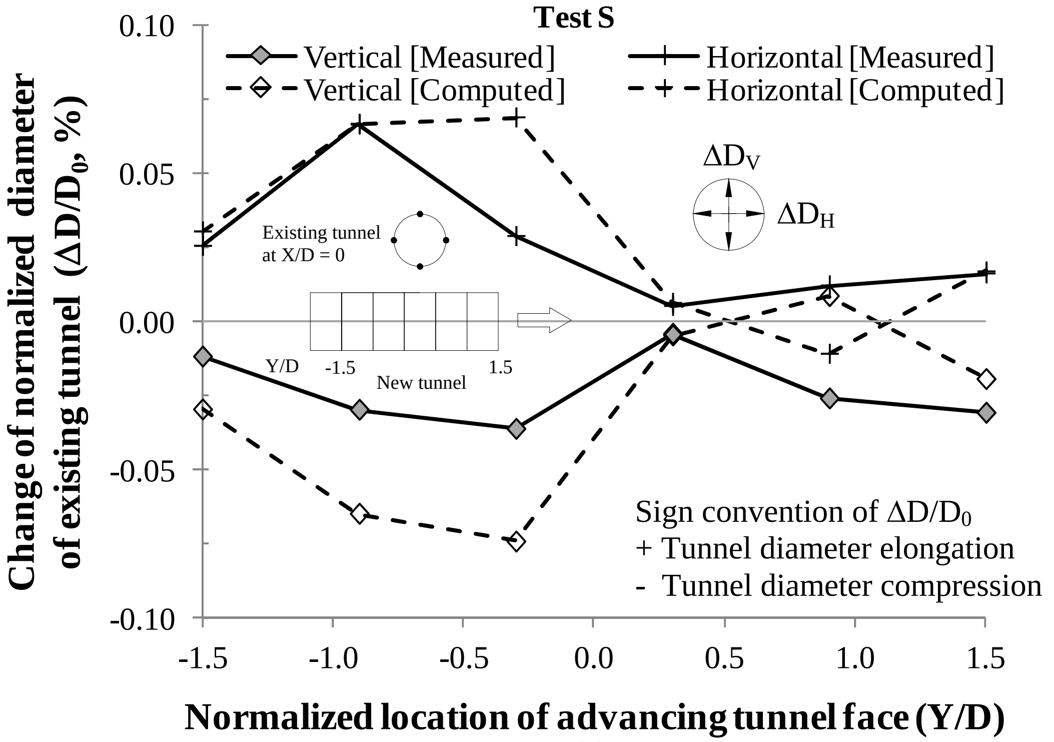

(a)

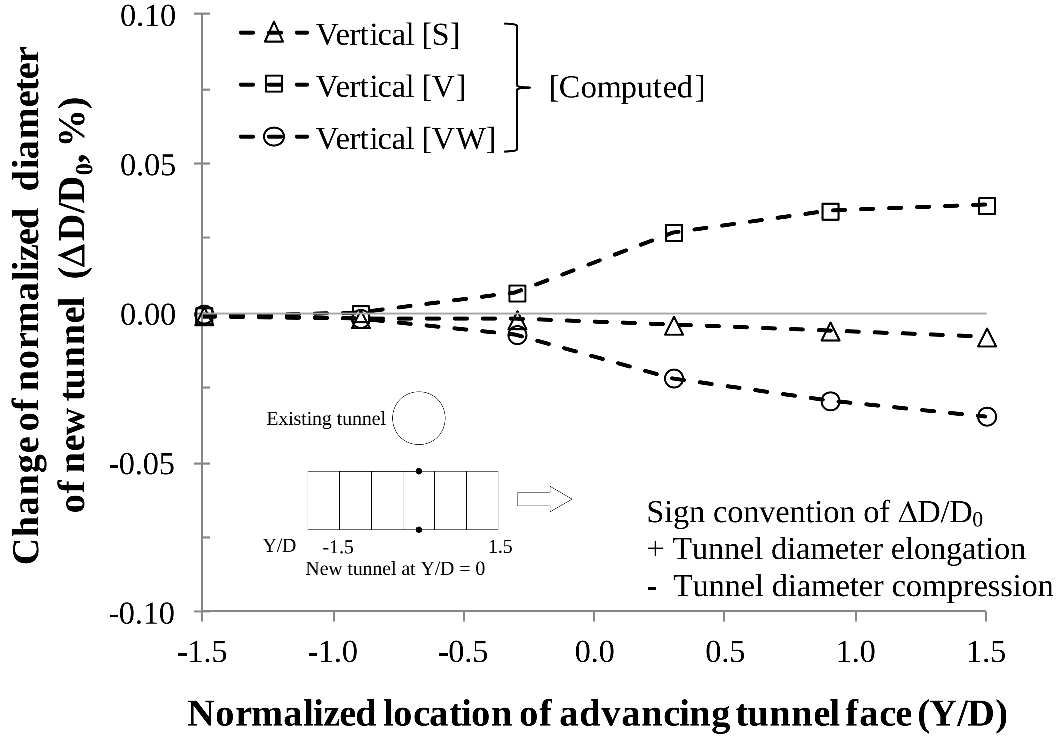

(b)

Figure 8 Deformations of (a) the existing tunnel in Test S; (b) the new tunnel in case S, V and VW

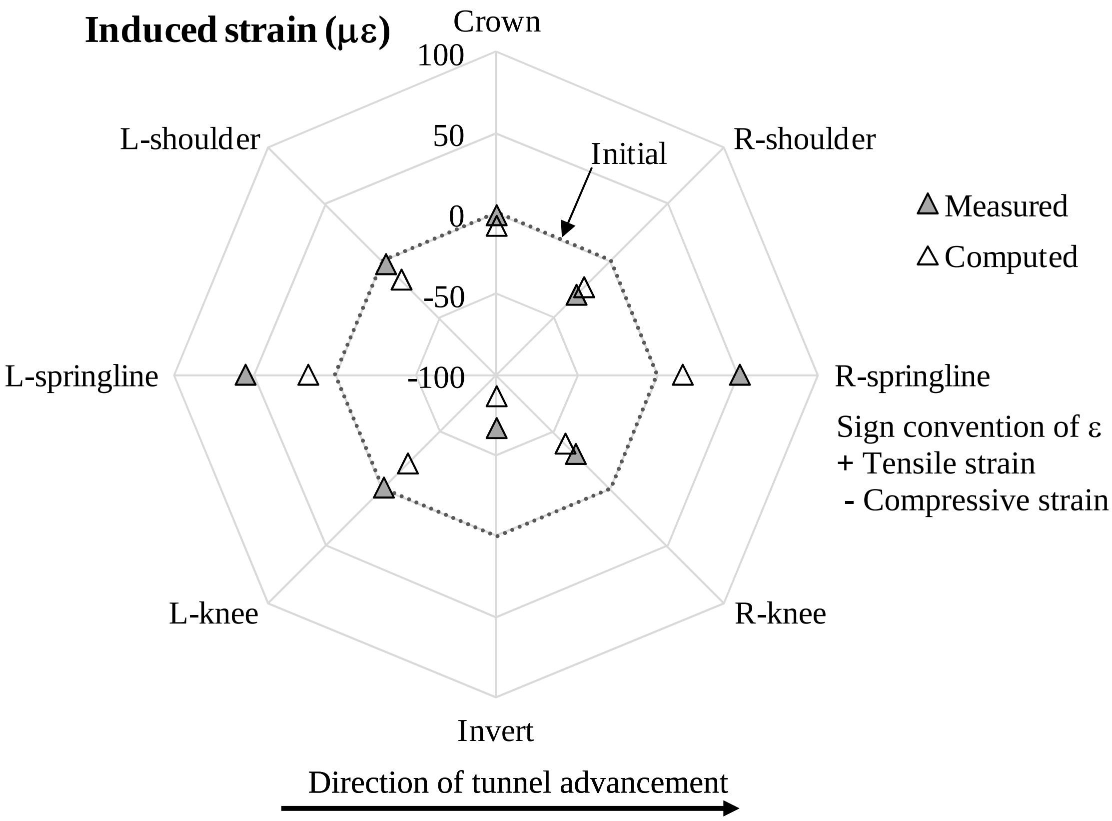

Figure 9 Induced strains at the outer face of the existing tunnel in the transverse direction in Test S

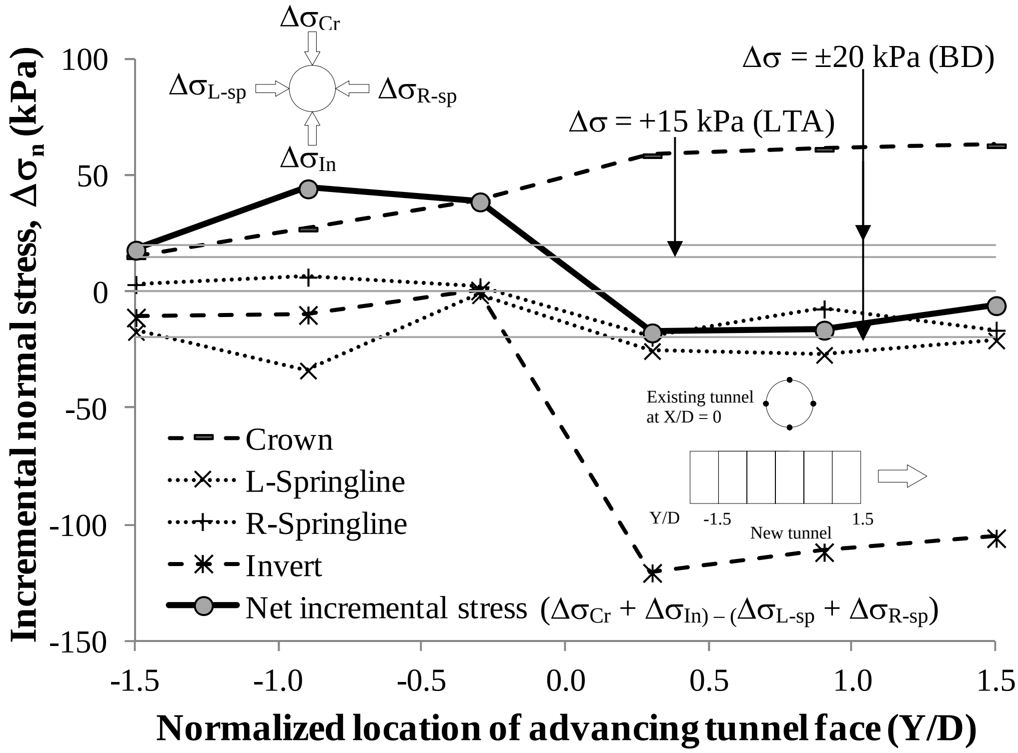

(a)

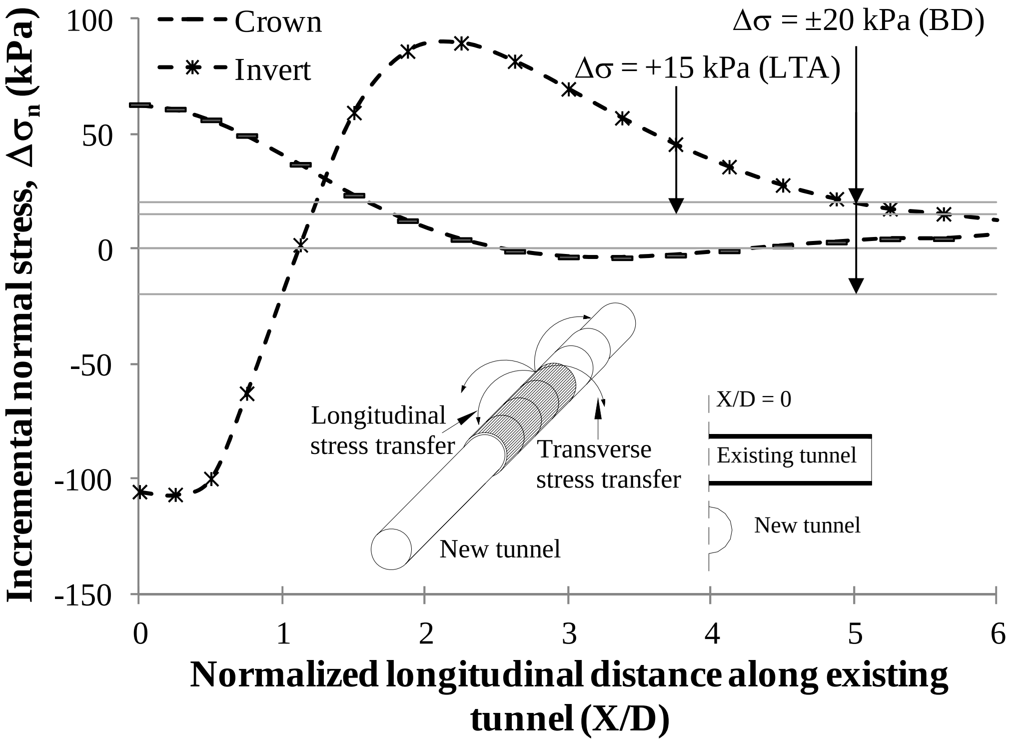

(b)

Figure 10 Computed incremental normal stresses at different key locations of the existing tunnel in case S in (a) the transverse direction during tunnel advancement; (b) the longitudinal direction at the end of tunnel excavation

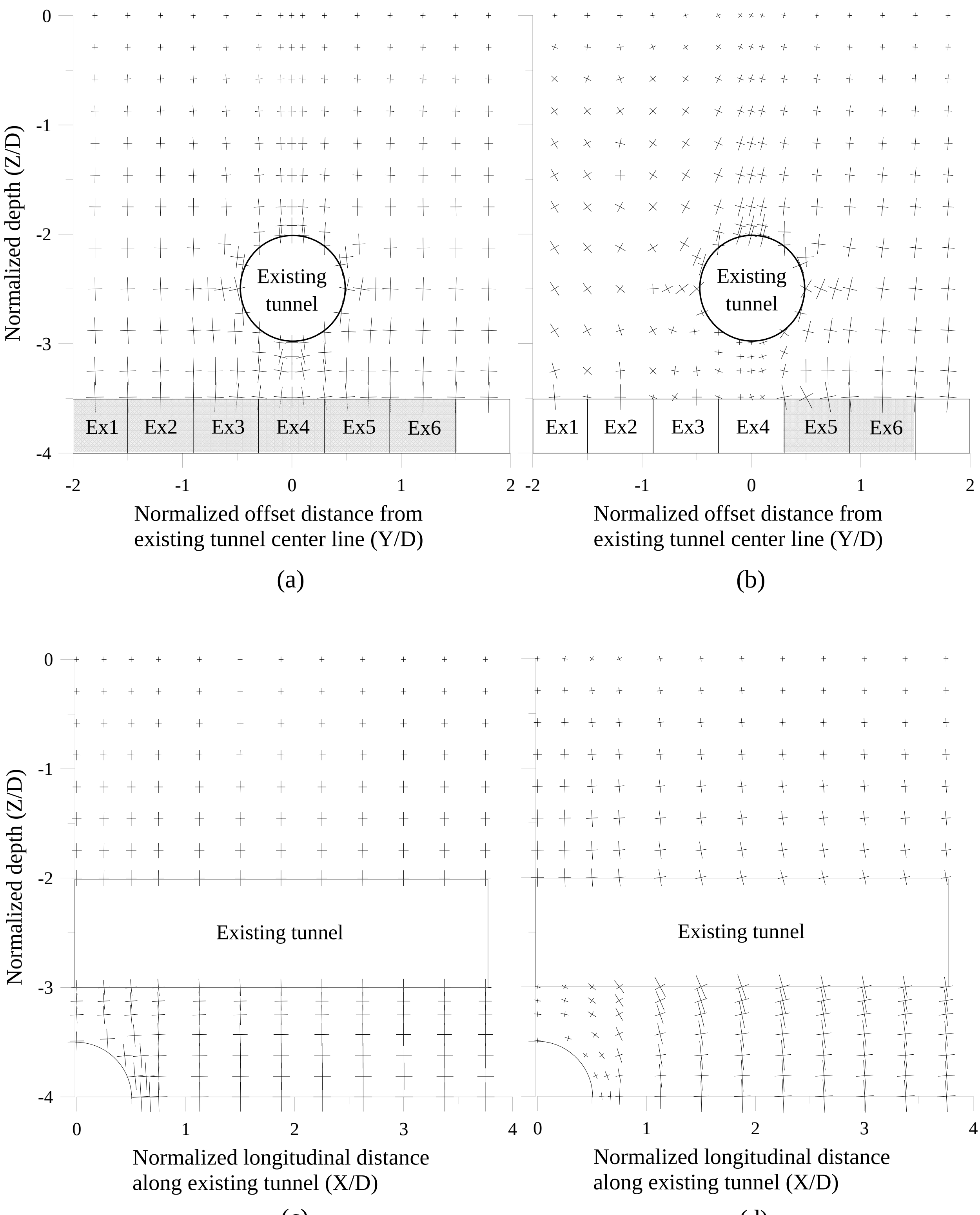

Figure 11 Computed directions of principal stress in case S in (a) the transverse direction before tunneling; (b) the transverse direction when the new tunnel reached Ex4; (c) the longitudinal direction before tunneling; (d) the longitudinal direction when the new tunnel reached Ex4

Table 1 Some relevant scaling laws for the centrifuge tests (Taylor, 1995)

Parameter	Unit	Scaling law (model/prototype)
Gravity	m/s^2	N
Length	m	1/N
Area	m^2	$1/N^2$
Volume	m^3	$1/N^3$
Density	kg/m^3	1
Unit weight	N/m^3	N
Flexural stiffness per unit width	$N \cdot m^2/m$	$1/N^3$
Flexural stiffness	$N \cdot m^2$	$1/N^4$
Stress	N/m^2	1
Strain	-	1

Table 2 Modeling sequences of new tunnel advancement in Tests S and VW

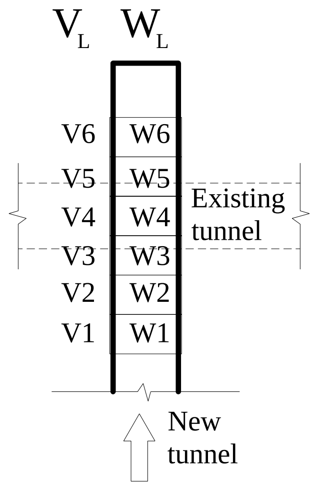

Modeling sequences		
S	**VW**	
V_1+W_1	V_1	⇧
V_2+W_2	V_2	
V_3+W_3	V_3	
V_4+W_4	V_4	**V**
V_5+W_5	V_5	
V_6+W_6	V_6	⇩
	W_1	⇧
	W_2	
	W_3	
	W_4	**VW**
	W_5	
	W_6	⇩

Table 3 Summary of material parameters adopted in finite element analyses

Critical state friction angle[a], ϕ_c	30°
Granulates hardness[a], h_s	2.6 GPa
Exponent n[a], n	0.27
Minimum void ratio at zero pressure[a], e_{d0}	0.61
Critical void ratio at zero pressure[a], e_{c0}	0.98
Maximum void ratio at zero pressure[a], e_{i0}	1.10
Exponent α[b], α	0.14
Exponent β[b], β	3.0
Parameter controlling the initial shear modulus upon 180° strain path reversal and in the initial loading[b], m_R	8
Parameter controlling the initial shear modulus upon 90° strain path reversal[b], m_T	4
The size of the elastic range[b], R	0.00002
Parameter controlling rate of degradation of stiffness with strain[b], β_r	0.1
Parameter controlling rate of degradation of stiffness with strain[b], χ	1.0
The coefficient of at-rest earth pressure, K_0	0.5

Note: (a) Herle & Gudehus, 1999
(b) Justify based on previous literatures (Maeda and Miura, 1999; Yamashita et al., 2000)

Table 4 Summary of case histories of crossing tunnels

	Heathrow Express Tunnels underneath Piccadilly Line Tunnels (Cooper et al., 2002)	**Shekou Line Tunnels underneath Luobao Line Tunnel** (Li & Yuan, 2012)
Project location	London	Shenzhen
Soil type	London Clay	Highly decomposed granite
Estimated K_0 at the depth of the existing tunnel axis	1.7[(a)]	0.4[(b)]
Dimensions of existing tunnel, $\mathbf{D_E}$ (m)	4.1 (Outer diameter)	6.8 (Width) x 13.6 (Height)[(c)]
Lining thickness of existing tunnel (m)	0.15	0.80
Outer diameter of new tunnel, $\mathbf{D_N}$ (m)	9.1	6.3
Cover depth of existing tunnel, $\mathbf{C_E}$ (m), [C_E/D_N]	11.0 [1.2]	15 [2.4]
Cover depth of new tunnel, $\mathbf{C_N}$ (m), [C_N/D_N]	21.5 [2.4]	30 [4.8]
Pillar depth, **P** (m), [P/D_N]	7.0 [0.8]	2.0 [0.3]
Skew of tunnel crossing angle, **S**	69^0	55^0
Tunnel excavation method	Pilot shield with tunnel enlargement	EPB shield
Volume loss reported (%)	1.3 – 2.5	Not available

Note: (a) Estimated from Hight et al. (2007)
(b) Adopted from Viana da Fonseca et al. (1997)
(c) Outer dimension of double deck existing tunnel